10.1   **MONITORING SURFACE WIND STRUCTURE WITH SPACEBORNE SAR:**
Development of a SAR User Guide

Robert C. Beal*
SSARGASSO, Ellicott City, MD

1. OVERVIEW

High resolution wide-swath SAR-derived wind fields over the ocean offer the potential for a new and unique perspective of the spatially evolving wind field, especially within storms and along coasts. SAR wind fields often show a spatial variability neither modeled nor measured by other methods. The SAR wind estimates are not error-free, of course, themselves containing systematic, random, and even nonlinear errors not yet fully understood. Even so, our present knowledge of the SAR error structure is sufficiently accurate to produce a unique potentially operationally useful high resolution wind product.

Supported by NOAA/NESDIS, collaborators from several institutions (Beal *et al.*, 2003) are teaming to produce a SAR Wind User's Guide. The Guide, currently planned for completion by December 2003, is built around a set of 60 Radarsat wide swath (430 km) passes acquired over the Gulf of Alaska and Bering Sea between 31 October 1999 and 14 November 2001. The structure of the Guide is briefly outlined here, along with an example from the Guide depicting one of the particularly interesting Radarsat passes from the set of 60.

2. RADAR BACKSCATTER TO SAR WIND

The starting point for all Radarsat SAR wind estimates included in the Guide is the JHU/APL algorithm based on the well documented (but flawed) CMOD4 relationship, and modified for HH polarization (Monaldo *et al.*, 2001). The accuracy of the estimates is suggested by Figure 1 (also from Monaldo *et al.*, 2001) which shows a scatter plot for 260 SAR-vs-buoy wind comparisons obtained mostly in the NW Atlantic during the winter of 1999-2000. For SAR off-nadir angles from 25˚ to 45˚, the standard deviation of the differences was 1.7 m/s for buoy wind speeds up to 21 m/s. For this com-

parison, the assumed local wind direction was taken from the model, usually within 6 hrs of overpass time. In some situations, this assumption can lead to significant errors in the SAR backscatter-to-wind transformation, and no doubt is the source of at least some of the scatter in Figure 1.
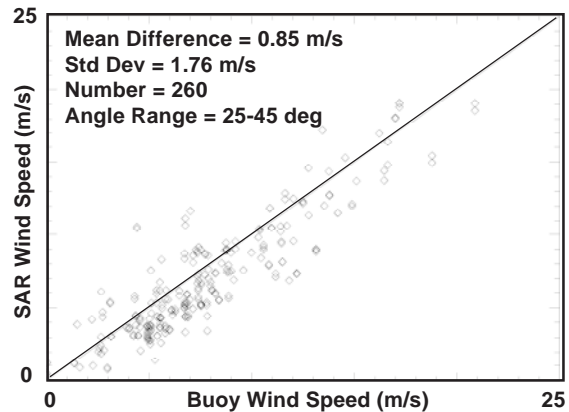
Figure 1: SAR vs Buoy Comparison
(from Monaldo *et al.*, 2001)

Recent reanalysis of Radarsat wind fields using QuikSCAT wind directions to drive the SAR algorithm indicates that the Radarsat wind errors may be <1 m/s when the initial wind direction error is small, at least up to winds of 20 m/s (Thompson *et al.*, 2001).

3. STRUCTURE OF THE GUIDE

Nearly all of the SAR passes chosen for detailed examination in the Guide contain regions of high (SAR-estimated) winds, generally exceeding 15 m/s. High wind passes have been selected specifically because they would be most interesting in operational applications.

The spatial distribution of the 60 Radarsat wind estimates included in the Guide is shown in Figure 2. The ScanSAR frames (typical dimension 430 km across-track by 500 km along-track) are concentrated in the Gulf of Alaska and Bering Sea. Many of the frames transect coastal areas, and reveal the rich variety of topographical influences on the surface wind that would be impossible to capture in

---

* *Corresponding Author Address:* Robert C. Beal, SSARGASSO Associates, 12222 Carroll Mill Road, Ellicott City, MD 21042; e-mail: rcbeal@aol.com or r.beal@jhuapl.edu.
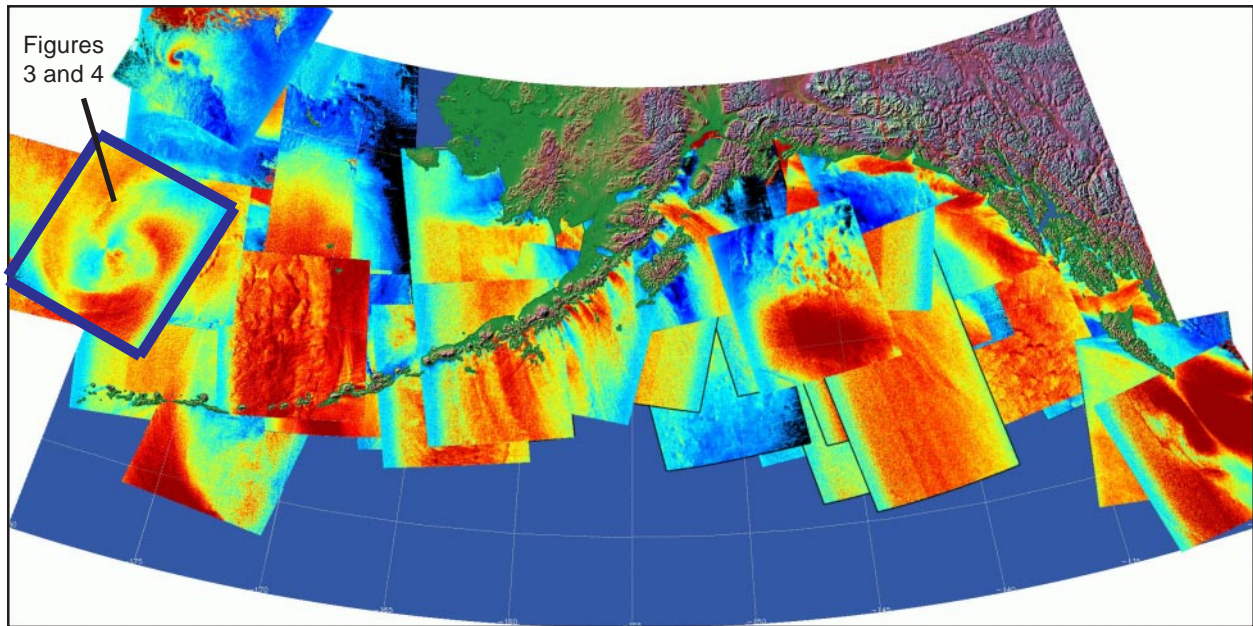
Figure 2: Spatial distribution of 60 Radarsat passes in the Gulf of Alaska and Bering Sea
31 October 1999 to 14 November 2001

such detail by any other method, i.e., by either an instrument or a computer model.

Section I of the Guide (Introduction and Overview) gives its purpose, including a description of the present status and future potential of wide swath SAR for wind field analysis and interpretation. This section is expected to cover a) future operational potential, b) methodology (including such things as averaging kernels, interpolation methods, measurement uncertainties, and potential error sources), and c) the physical basis and behavior of the SAR wind algorithm.

Section II (Meteorological Phenomena in High Resolution SAR Wind Imagery) contains a description of the variety of meteorological phenomena commonly found in SAR wind imagery. This section is partitioned according to the 11 distinct classes of meteorological phenomena identified in the imagery: 1) island and mountain wakes, 2) point wakes, 3) mountain lee waves, 4) simple gap flows, 5) hybrid gap flows (including both reverse gap flow and gap flow/synoptic interaction), 6) synoptic fronts, 7) synoptic lows, 8) mesoscale lows along fronts, 9) mesoscale lows associated with cold air outbreaks, 10) convection, and 11) coastal barrier jets. Examples of each of the 11 categories are drawn from an image inventory contained in Section III, further elucidated below.

In the Section III image inventory, a standard format is employed to aid the interpretation and to allow easy cross-comparison among SAR wind fields from different passes. One of the more interesting pass-pairs (from 06 December 2000) is described in Figures 3 and 4, which contain a synoptic description in a (temporally and spatially) wide region surrounding the SAR acquisition, as deduced from a numerical model (U.S. Navy Fleet Numerical NOGAPS) perspective. The first four panels (a-d) depict the evolving surface pressure field during the ~36 hrs prior to acquisition. The next four panels (e-i) contain other relevant (some potentially algorithm-contaminating) parameter fields: surface winds, surface wave height, surface inverse wave age (ratio of the vector wind speed to the vector wave phase velocity), which is a measure of the wave steepness of the dominant wave system, and the air-minus-sea temperature, which is a measure of the Marine Atmospheric Boundary Layer (MABL) stability. These last two parameters, both potentially important to understanding some of the error sources of SAR wind estimates, are derived from other model parameters. Finally, the model surface wind field within the highlighted region of the first 8 panels is expanded in a gnomic projection (i) with the SAR wind frame(s) overlaid. Figure 4 focuses specifically on the high resolution (300 m pixel [except in this reduced version, closer to ~1 km]) SAR wind estimates, in the context of model winds.

a) Pressure (mb) ~ t_0-36h **b) Pressure (mb) ~ t_0-24h** **c) Pressure (mb) ~ t_0-12h** **d) Pressure (mb) ~ t_0**

960 — 1040   960 — 1040   960 — 1040   960 — 1040

e) Surf Wind Field (m/s) ~ t_0 **f) Surf Wave Height (m) ~ t_0** **g) Inverse Wave Age ~ t_0** **h) Air-Sea Temp (°C) ~ t_0**

0 — 25   0 — 8   -1 — +2   -10 — +10
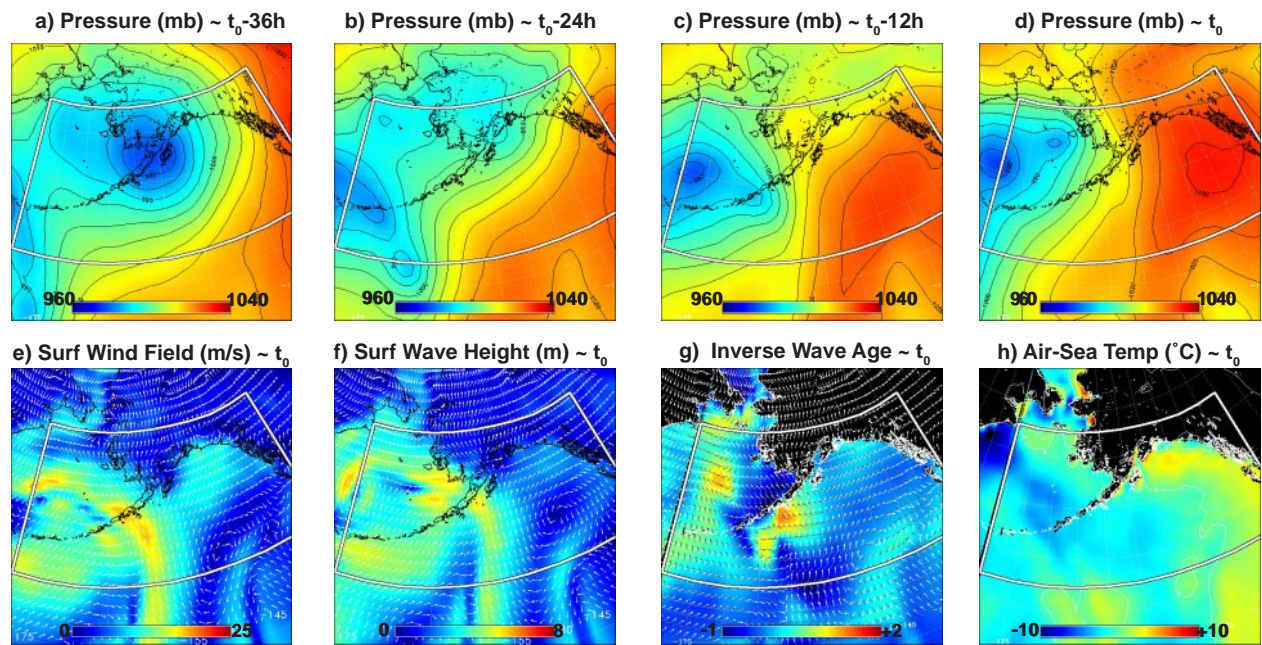
**i) Model Wind Field
for 1800 GMT 06 Dec 2000
with embedded SAR overpass at 1818 GMT**

170W   160W   150W   140W

60N   60N

MRKA2
POTA2
BLIA2
46060
46061

FFIA2

46035

55N   55N

46001

50N   50N

46003

0   Wind Speed (m/s)   25

170W   140W
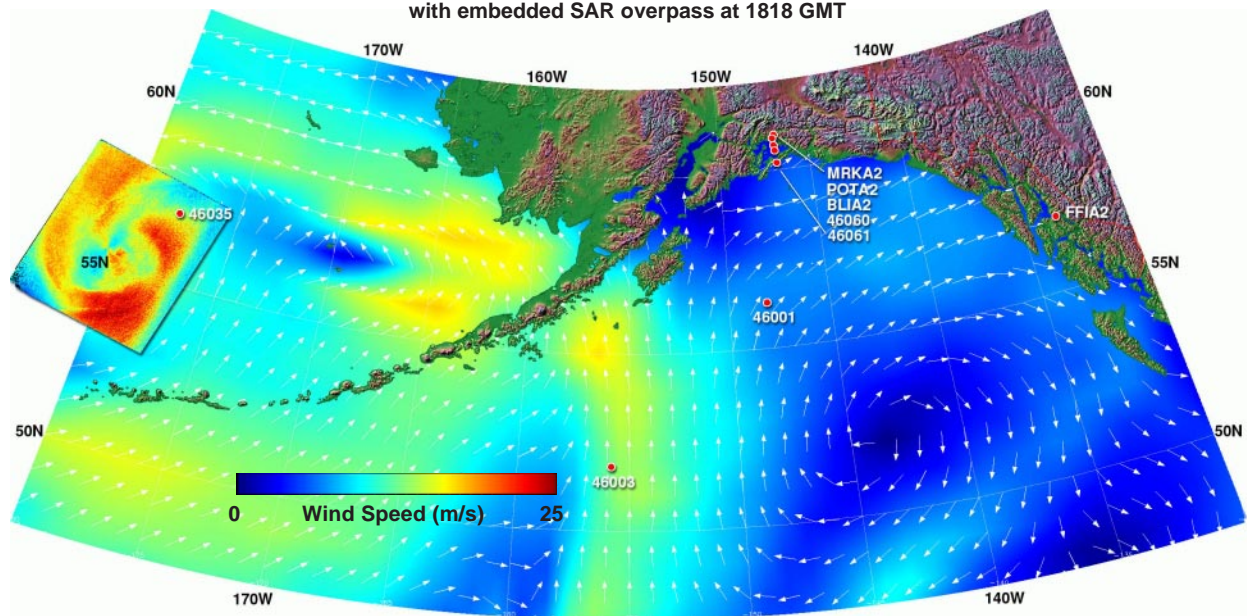
Figure 3 (Model): As the low of the previous day (05 Dec) dissipates over central Alaska, another strengthens over the central Bering Sea (a-d), producing a tight, nearly circularly symmetric wind field with a long arm of high winds stretching eastward over the Alaska Peninsula and then southward through the Gulf of Alaska (e, i). Highest waves are in the western sector of the storm (f), but are more fully developed (steeper) in the eastern sector (g). The MABL is unstable in all sectors (h).

Enlarged SAR Frame
Radarsat ScanSAR B Wind Field
SAR Time: 1818 GMT 06 Dec 2000
Model Time: 1800 GMT 06 Dec 2000
Frame Dimension: 430 km x 500 km
Pixel dimension: 300 m (~1 km here)

Wind Speed (m/s) 0 — 30

Scale (km) 0 — 200
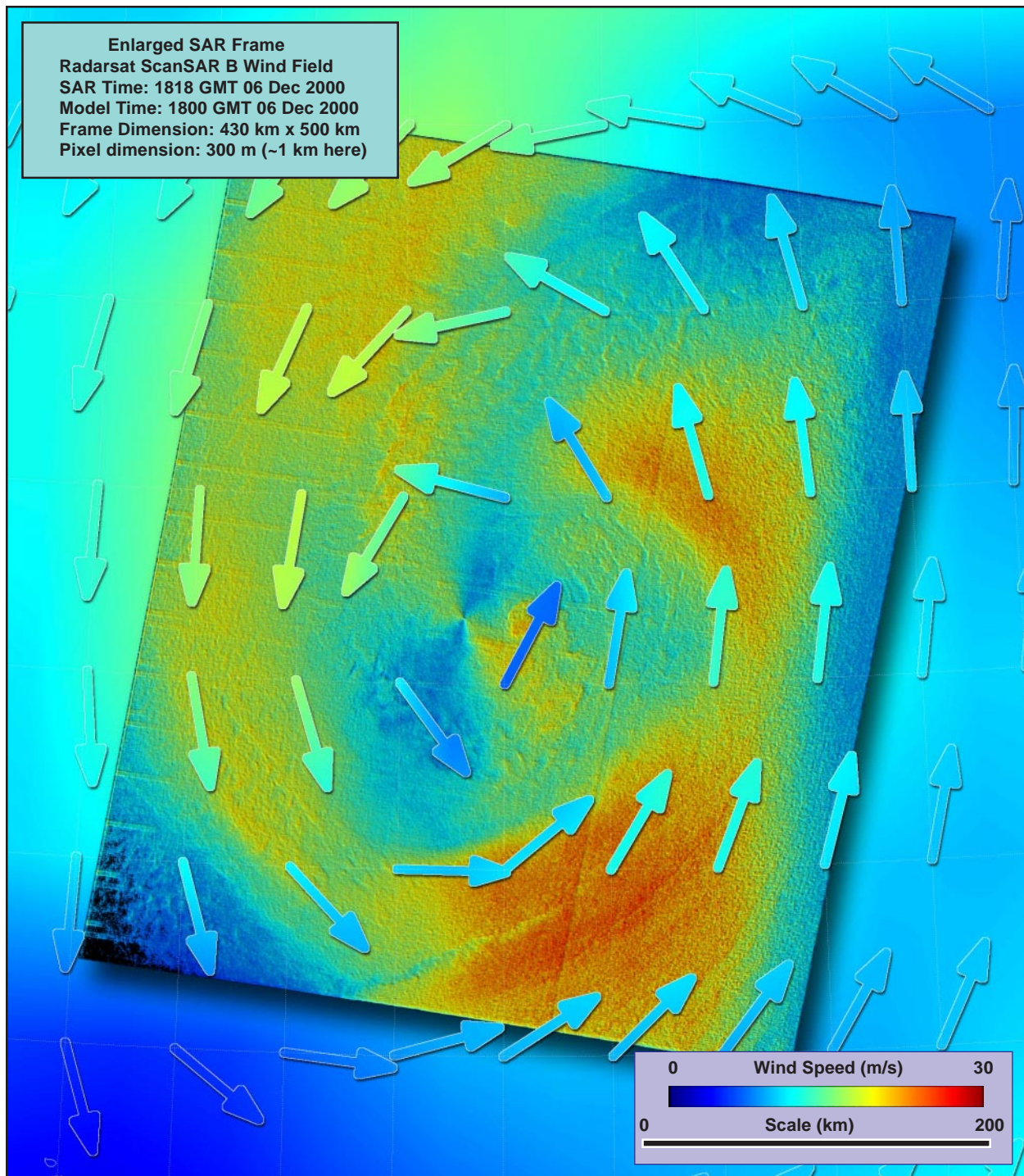
Figure 4 (SAR): Both the SAR and the model (magnitude-coded arrows) beautifully capture the structure of the nearly symmetrical wind field, but the SAR reveals a more complex morphology. Even though the SAR wind estimates are slightly high with respect to the model, the morphology revealed by the SAR is doubtless more accurate than that from the model. Note the slight expansion of the wind scale from 25 m/s in Figure 3 to 30 m/s here. The original 300 m pixel size has been degraded here to ~1 km to reduce file size. (Higher resolution version is available at URL http://fermi.jhuapl.edu/sar/stormwatch/user_guide/.)

4. PRELIMINARY RESULTS

Many of the comparisons shown in the Guide indicate that there are still some large errors associated with the SAR wind estimates, at least those produced from the Alaska SAR Facility. The error appears to become more significant at winds above about 15 m/s. Although the error is difficult to characterize with a limited data set, it appears to result in large part from a nonlinear (wind-dependent) discontinuity in the SAR response at a fixed off-nadir angle that produces as much as a 5 m/s positive bias above 15 m/s. The SAR yields somewhat low estimates at low off-nadir angles countered by high estimates at medium to high off-nadir angles.

The bulk of these errors (or biases) are probably caused by a combination of 1) ground station processor errors (all 60 passes were processed at the Alaska SAR Facility in Fairbanks), 2) instrument calibration errors and nonlinearities, 3) inadequate characterization of the wind algorithm by CMOD4, especially at low off-nadir angles and/or high wind speeds, and 4) errors in the assumed model wind directions, necessary to deduce a unique wind speed from the radar backscatter. Residual scatter from other sources, such as atmospheric stability, ocean wave steepness (or inverse wave age), and surface contaminants, appear to be masked by the first four, at least at high wind speeds.

Nevertheless, and especially in the vicinity of storms, fronts, and coastal regions, the SAR is clearly revealing a much more complex structure to the local wind field than either the models or other remote sensors. With the instrument improvements expected in the European ENVISAT Advanced Synthetic Aperture Radar (ASAR), this advantage will become even more clear.

5. REFERENCES

Beal, R. C., F. M. Monaldo, D. R. Thompson, N. Winstead, G. S. Young, C. Scott, "High Resolution Wind Monitoring with Wide Swath SAR: A User's Guide", anticipated completion Dec 2003. (URL: http://fermi.jhuapl.edu/sar/stormwatch/user_guide/).

Monaldo, F. M., D. R. Thompson, R. C. Beal, W. G. Pichel, and P. Clemente-Colón, "Comparison of SAR-Derived Wind Speed with Model Predictions and Ocean Buoy Measurements", *IEEE Trans. Geosci. Remote Sensing*, vol. 39, pp.2587-2600, Dec 2001.

Thompson, D. R., F. M. Monaldo, W. G. Pichel, and P. Clemente-Colón, "Combined Estimates Improve High-Resolution Coastal Wind Mapping", *EOS Trans. AGU*, vol. 82, p. 469, Oct 2001.

6. ACKNOWLEDGEMENT